JOURNAL OF GUIDANCE, CONTROL, AND DYNAMICS
Vol. 19, No. 3, May–June 1996

H_∞ Control of an Earth Observation Satellite

Sandrine Le Ballois*
IUP Génie Électrique, 95033 Cergy, France
and
Gilles Duc†
École Supérieure d'Électricité, 91192 Gif-sur-Yvette, France

Results of a research program to design a high-performance attitude control system for an Earth observation satellite are presented. The controller is designed using the H_∞ coprime factorization approach. Two steps are necessary to perform the synthesis: a classical loop shaping and an H_∞ robust stabilization. A continuous time controller is first designed. Robustness against parameter uncertainties is then checked using mixed real/complex μ analysis. Last, a discrete time synthesis is performed to provide the controller to implement. The same loop shape is used in continuous time as in discrete time. Results concerning the implementation of the controller in a nonlinear simulation are detailed.

I. Introduction

A REVIEW of the new problems encountered in space control[1,2] has revealed that space structures pose a challenging problem in control design. In the face of large modeling uncertainties, the requirements in precision have continued to increase. For that reason the French space agency, the Centre National d'Études Spatiales (CNES), has been involved since 1990 in a program to assess potential benefits of new guidance, navigation, and control concepts based on modern robust control theory.

The focus is on the Earth observation satellite, Satellite Pour l'Observation de la Terre (SPOT), attitude control because it includes many interesting generic problems: a lot of flexible modes (because of a large solar array), badly known flexibility, low damping, multiaxis coupling, disturbances, etc.

Among the techniques that have been used are linear quadratic Gaussian (LQG) control, combined with loop transfer recovery and frequency shaping. These methods have given satisfactory results compared to classical control techniques, especially for the rejection of the external disturbances. However, the new controllers have been synthesized for one given position of the solar array. Controller changes are necessary for the other positions. Moreover, the new controllers have about 16–19 state variables, whereas the classical controller has only 6. This solution is not acceptable for an onboard computer where memory is very limited.

Because of this drawback, and because H_∞ methods offer a general context for a frequency domain formulation of performance and robustness objectives, CNES decided to focus on a detailed evaluation of such methods for future phases of the study. The evaluation was performed by the Control Department Laboratory of École Supérieure d'Électricité[3,4] (Supelec), and this paper presents the current results of this research.

In Sec. II, the problem is presented together with the satellite description and design specifications. A summary of the coprime factors based H_∞ synthesis[5] selected for the design is reviewed in Sec. III. A controller is synthesized in Sec. IV with special emphasis on the two-step decomposition: 1) a classical loop shaping and 2) a H_∞ robust stabilization. Linear simulation results and mixed real/complex μ analysis of the robustness are presented. In Sec. V, a discrete version of the controller is implemented in a nonlinear simulation. Results are given to analyze the disturbance rejection and the behavior throughout one orbit, using different values of the plant parameters.

Received March 27, 1995; revision received Nov. 9, 1995; accepted for publication Dec. 13, 1995.

*Associate Professor, 8 le Campus.

†Professor, Service Automatique.

II. Problem Presentation and Design Specifications

Problem Presentation

The SPOT satellites (Fig. 1) are dedicated to Earth observation. Pictures of the Earth are taken and all of the collected data are transmitted to a center specialized in image processing. These pictures interest a great variety of users: cartographers, geologists, farmers, etc.

Taking such photographs with high resolution, 10 m from an altitude of 832 km, requires very efficient control laws to maintain the satellite angular position within the requested pointing precision. The controller has to face external disturbances (gravity gradient, aerodynamic pressure, solar pressure, etc.) and internal ones [flexibility of the solar array, solar array drive motor (SADM) harmonics, moving parts, etc.].

SPOT4 has three different operating modes: 1) a fine pointing mode involving reaction wheels as actuators, 2) a coarse pointing mode involving thrusters as actuators, and 3) a survive mode used only if a computer failure occurs.

The present study focuses on the fine pointing mode, which is also the normal mode. The main difficulty is the coupling between the flexible solar array and the central body. It introduces a lot of flexible modes inside and outside the bandwidth with very low damping. This problem is complicated by the rotation of the solar array, which involves a modification of dynamics: flexible modes are exchanged between Y and Z axes. Table 1 sums up the critical items and control requirements.

Mathematical Models of the Satellite

A simplified model is first derived directly from mechanical equations: the platform of the satellite is viewed as a rigid body, whereas

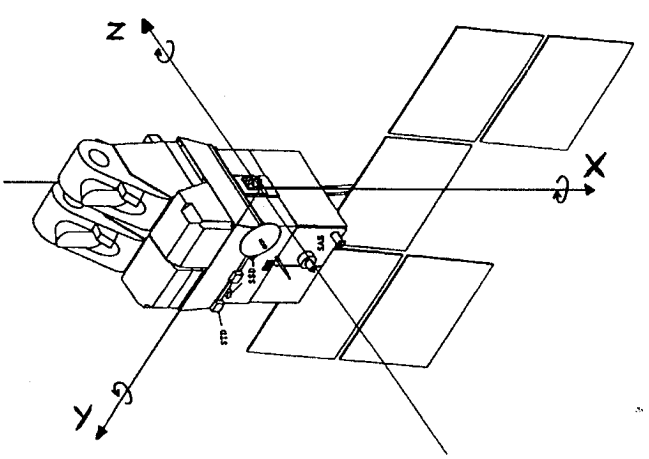

Fig. 1 SPOT4.

Table 1 SPOT4 in fine pointing mode

Critical points		Control requirements
External and internal disturbances	⇒	High gain at low frequencies
Uncertain flexible modes	⇒	Robust control
Solar array varying configuration	⇒	Scheduled or robust control
Coupling between axes	⇒	Multivariable control

the solar array is considered a flexible appendage. The basic simplification is that the SADM is a part of the platform and does not introduce any additional stiffness. This model, which is linear and is used for designing the control law, will be presented subsequently.

Linear models, more complete than the previous one, are also available from the software DYCEMO developed by Matra Marconi Space (MMS). For a first evaluation of the design, the linearized models for different operating points are used for the simulations, using MATLAB/SIMULINK.

Finally a very complete model of SPOT4 exists with all of the nonlinearities and including most of the parameters of the spatial environment (solar pressure, gravity gradient, etc.). Such a model is useful for a high-level validation of the designed control law: the operating conditions are similar to the ones the satellite could find on its orbit. This model is available from the software SPL developed by MMS.

The simplified linear model is given by

$$I_G\ddot{\theta}_G + L_G^T\ddot{\eta} = C_{\text{ext}} \tag{1}$$

$$\ddot{\eta} + C\dot{\eta} + K\eta = -L_G\ddot{\theta}_G \tag{2}$$

where C_{ext} is the external torque vector, θ_G is the satellite attitude angle vector, L_G is the modal participation matrix, I_G is the inertia matrix, η is the flexible modes state vector, C and K are diagonal matrices with $C_{ii} = 2\zeta_i\omega_{ci}$ and $K_{ii} = \omega_{ci}^2$, where ζ_i and ω_{ci} are the damping and the natural frequency of mode i.

Equations (1) and (2) are rearranged to give a state–space representation of the plant:

$$\dot{x} = Ax + Bu \tag{3a}$$

$$y = Cx + Du \tag{3b}$$

where the state vector $x \in R^{22}$ includes the three satellite attitude angles and their three derivatives, the eight flexible modes state vector and their eight derivatives; the control variable $u \in R^3$ includes the three torques at the centerbody generated by reaction wheels; the measurement $y \in R^3$ includes the three angular rates at the center body determined by rate gyro sensors.

Disturbances

Two disturbances are considered. The enregistreur magnétique spatialisé (EMS) disturbance is representative of the transient input torque disturbance occurring when the video recorder starts. It is shown in Fig. 2.

The second disturbance is sensor noise. Its power spectral density is limited to half of the sampling frequency. It is given in degree per hour squared by

$$S(f) = \tfrac{1}{2}\left[\left(a_0/f^2\right) + a_1 + a_2 f^2\right] \tag{4}$$

with f in hertz, where $a_0 = 4.8 \times 10^{-9}$, $a_1 = 4.46 \times 10^{-3}$, and $a_2 = 5.8 \times 10^{-3}$.

The main characteristics of the problem are, therefore, a 22-state model, with eight flexible modes located from 0.76 to 18.5 rad/s, with 5×10^{-4} damping, three reaction wheels as control actuators, three rate gyros as sensors, and two disturbances.

In addition, model uncertainties have to be considered. The controller must stabilize the plant despite about ±30% uncertainty in the natural frequency of the flexible modes. Finally, the rotation of the solar array also provides a modification of the natural frequencies (see Fig. 3).

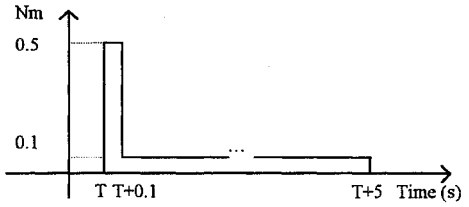

Fig. 2 EMS disturbance.

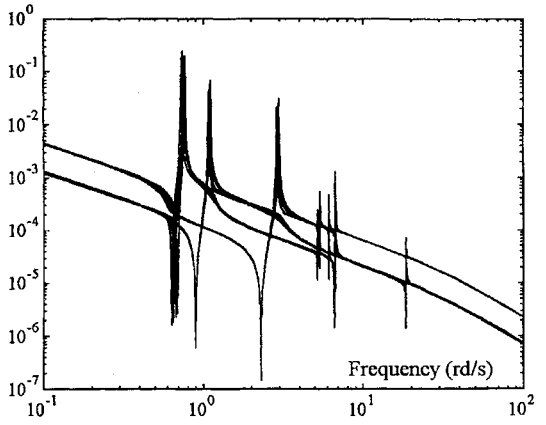

Fig. 3 Singular values of the plant for five panel positions from 0 to 180 deg.

Design Specifications

The angular positions and rates are to be regulated to zero. The controller must robustly stabilize the plant despite all of the aforementioned uncertainties. A unique controller should be designed for all of the positions of the solar array. Settling time, angle rejection, and rate rejection to an EMS disturbance have to be less than 12 s, 12×10^{-5} rad, and 4×10^{-5} rad/s, respectively. Rate rejection to gyro noise has to be less than 2×10^{-6} rad/s. Maximal absolute value of the control torque has to be less than 0.45 Nm.

III. H_∞ Control Methods

Introduction

Since the pioneering work of Zames,[6] emphasis has been placed on the development of H_∞ control theory. Two different approaches are commonly used. On the one hand, a method based on closed-loop specifications has been developed, and Doyle et al.[7] have stated the formulas for obtaining the controller. This method is known as the closed-loop or state–space approach, and the solution needs the resolution of two γ-dependent Riccati equations. On the other hand, a method based on open-loop specifications has been developed by McFarlane and Glover[5] and is known as the coprime factors approach.[8] Since this method does not address performance directly, it is connected with a loop shaping procedure. No γ iteration is required and the solution is given by the resolution of two LQG type Riccati equations.

Choice of the Method

The latter method has been chosen for the present design since it is known to have interesting properties. First, the Riccati equations are numerically better conditioned than the γ-dependent Riccati equations of the state–space approach. Moreover the optimal value of the H_∞ criterion is known a priori. Furthermore, this method avoids exact pole/zero cancellations between the plant and the controller.[9] This latter property is interesting when the controlled plant has flexible modes. Last, formulas are available to perform a discrete synthesis directly[10,11] without using the bilinear transformation. This is a substantial advantage with respect to the state–space approach where the discrete solution is very difficult to compute.[12]

Coprime Factors Robust Stabilization Problem

Continuous-time as well as discrete-time transfer matrices can be considered in the following. Let P_0 be the transfer matrix of the nominal plant to be controlled. A normalized left coprime factorization

of P_0 is given by $P_0 = \tilde{M}_0^{-1}\tilde{N}_0$, where $(\tilde{M}_0, \tilde{N}_0)$ are stable and proper transfer matrices such that

$$\tilde{M}_0\tilde{M}_0^* + \tilde{N}_0\tilde{N}_0^* = I \tag{5}$$

Considering additive uncertainties on each coprime factor, a family of perturbed plants can be defined as follows:

$$\boldsymbol{P}_\varepsilon = \left\{ P_\Delta = (\tilde{M}_0 + \Delta_M)^{-1}(\tilde{N}_0 + \Delta_N),\ \|(\Delta_M \quad \Delta_N)\|_\infty < \varepsilon \right\} \tag{6}$$

The robust design problem is to find a unique fixed controller K stabilizing all of the plants in the set $\boldsymbol{P}_\varepsilon$ (see Fig. 4).

This problem was shown to be a particular H_∞ problem

$$\inf_{K_{\text{stabilizing}}} \left\| \begin{pmatrix} K(I + P_0K)^{-1}P_0 & K(I + P_0K)^{-1} \\ (I + P_0K)^{-1}P_0 & (I + P_0K)^{-1} \end{pmatrix} \right\|_\infty = \varepsilon_{\max}^{-1} \tag{7}$$

The problem is equivalent to finding the largest ε, denoted $\varepsilon_{\max}$ and called the stability margin, for the set defined in Eq. (6). As an advantage of using normalized coprime factors, $\varepsilon_{\max}$ is known a priori to be

$$\varepsilon_{\max} = \sqrt{1 - \|\tilde{N}_0 \quad \tilde{M}_0\|_H^2} \tag{8}$$

where $\| \|_H$ denotes the Hankel norm.

Formulas involving the resolution of two LQG type Riccati equations are available to construct any controller achieving a value ε arbitrarily close to $\varepsilon_{\max}$. They are given for the continuous-time case[5,8] and for the discrete-time case.[10,11]

Loop-Shaping Procedure

Because no weighting matrix can be introduced in Eq. (7), one cannot specify explicitly the desired closed-loop performances. Thus, to increase the degrees of freedom and to address this concept, pre- and/or postcompensators W_1 and W_2 are introduced to shape the nominal plant. P_0 is, therefore, replaced by $P_s = W_2P_0W_1$, and the H_∞ robust stabilization is performed on P_s by solving

$$\inf_{K_{\text{stabilizing}}} \left\| \begin{pmatrix} K(I + P_sK)^{-1}P_s & K(I + P_sK)^{-1} \\ (I + P_sK)^{-1}P_s & (I + P_sK)^{-1} \end{pmatrix} \right\|_\infty = \varepsilon_{\max}^{-1} \tag{9}$$

This problem can be summarized by the block diagram of Fig. 5. The four transfer functions appearing in Eq. (9) are between inputs e_1, e_2 and outputs s_1, s_2. As an advantage of considering this problem, each will have a H_∞ norm limited by, at least, $\varepsilon_{\max}^{-1}$.

According to Fig. 5, W_1 and W_2 can be viewed as pre- and postfilters selected to give a particular shape to the plant before computing the H_∞ controller. Integral action is usually included in W_1 but one can add proportional gain for performance, or low-pass filters to increase the rolloff.

According to Eqs. (6) and (9), $\varepsilon_{\max}$ is simultaneously related to robustness and performance. It is, therefore, a useful indicator to design the compensators W_1 and W_2. Usual values of $\varepsilon_{\max}$ are between 0.3 and 0.5.

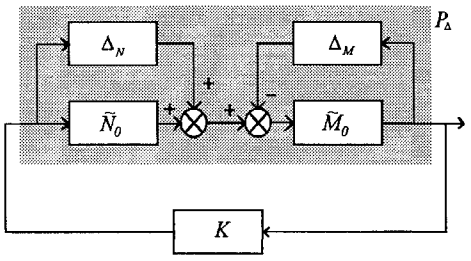

Fig. 4 Robust design problem.

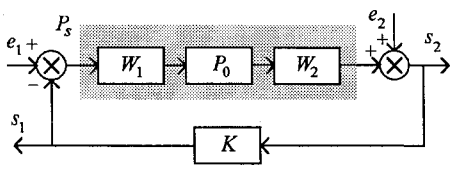

Fig. 5 Block diagram of the H_∞ problem.

IV. H_∞ Control Design

Introduction

A continuous-time synthesis has been conducted. This allows us to perform μ analysis to verify the robust stability with respect to uncertainties in the natural frequencies of the flexible modes. Using the same pre- and postcompensators as those defined in the continuous-time case, a discrete-time synthesis is performed.

Choice of the Model

The choice of the synthesis model is a very important point for the robust stability of the control law. It is necessary to introduce in the nominal model all of the a priori knowledge about the system to be controlled.

A kind of worst-case model has been chosen (see Table 2). By choosing an angle of 45 deg between the solar array and the platform, each of the three axes of the satellite is affected by all of the flexible modes (this is not the case at 0 deg). The natural frequencies of the modes have been chosen close to the desired bandwidth, which is between modes 2 and 3. The damping was chosen to be very small for safety reasons (for the simulations this constraint can be relaxed to $\zeta = 10^{-3}$).

Continuous-Time Synthesis

The basic problem is to control a flexible structure submitted to parametric uncertainties (the natural frequencies of the flexible modes). It is well known[6] that H_∞ techniques are not well suited if uncertainties are clearly parametrized. To shrink the uncertainty ball centered in the nominal plant, an inner loop is introduced. As explained by Zames,[6] feedback reduces the sensitivity to plant uncertainty. Furthermore, collocated feedback is a well-known technique to control flexible structures.[13,14]

The mentioned techniques are invoked here to introduce rate feedback prior to the loop shaping. The gain K_b (Fig. 6) is selected to ensure that the singular values of GK_b have a crossover frequency beyond the third flexible mode, i.e., the inner-loop bandwidth is greater than the specified bandwidth of the closed-loop system. This improves the damping of the first three flexible modes.

In the actual process, angular positions θ are obtained from rate measurements $\dot{\theta}$ by using an estimator. A very simple way to symbolize this estimator is to consider the following postcompensator applied to the output $\dot{\theta}$ of the plant:

$$W_2 = [(1/s) \times I_3 \quad I_3]^T \tag{10}$$

W_1 has the form $W_1 = (K_E \quad K_V)$, where K_E and K_V are 3×3 matrices that before applying the H_∞ controller K correspond to position and rate feedback, respectively. Choosing $K_V \ll K_b$ will slightly modify the inner loop, whereas K_E tunes the closed-loop bandwidth and the damping of the rigid-body modes. Selected values are the following:

$$K_b = \text{diag}\{-3181 \quad -2429 \quad -3533\} \tag{11}$$

$$K_E = \text{diag}\{1506 \quad 586 \quad 1249\}; \qquad K_V = I_3 \tag{12}$$

Table 2 Synthesis model

Synthesis model	Simplified dynamic
Solar array configuration	45 deg
Number of flexible modes	8
Damping of the flexible modes	$\zeta = 5 \times 10^{-4}$
Location of the flexible modes	ω_{c1}, ω_{c8}: nominal; ω_{c2}: +20%; ω_{c3}: −20%; ω_{c4}–ω_{c7}: −30%

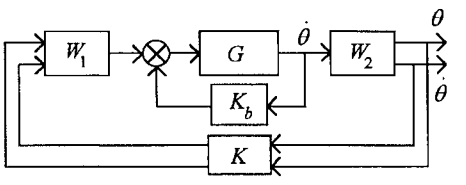

Fig. 6 Control structure: continuous-time synthesis.

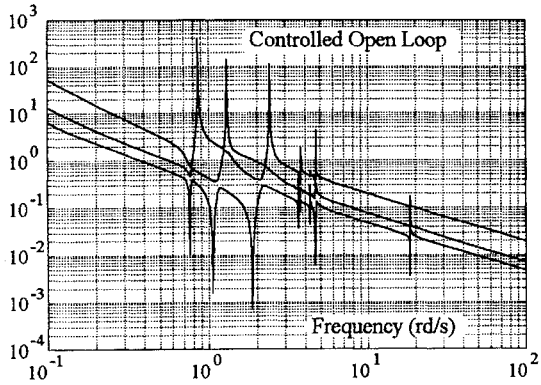

a) Singular values of GK_f

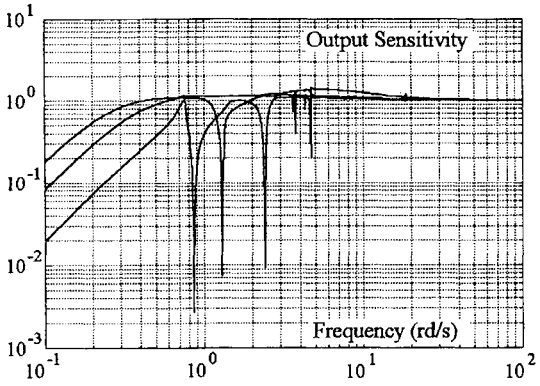

c) Singular values of $(I + GK_f)^{-1}$

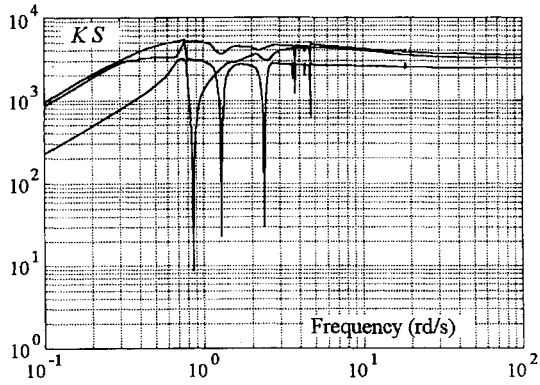

b) Singular values of $K_f(I + GK_f)^{-1}$

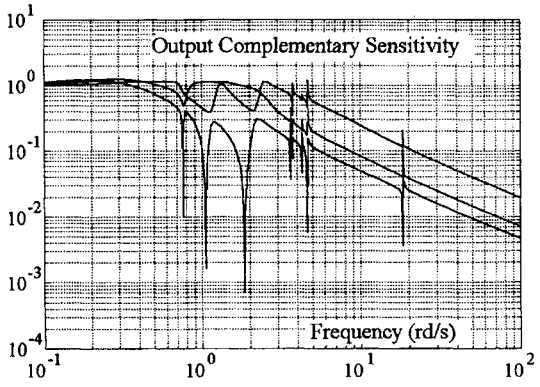

d) Singular values of $GK_f(I + GK_f)^{-1}$

Fig. 7 Frequency responses.

The maximum stability margin is then $\varepsilon_{\max} = 0.575$ and using the formulas available,[8] the controller is computed for $\varepsilon = 0.99\varepsilon_{\max}$. If the same compensators W_1 and W_2 are used without an inner loop, $\varepsilon_{\max}$ becomes equal to 0.38. This result shows that the rate feedback has decreased the uncertainty ball as expected.

Finally the control structure of Fig. 6 corresponds to an equivalent controller

$$K_f = (W_1 K W_2 + K_b) \tag{13}$$

which has 28 state variables.

Frequency Responses

Singular value Bode plots for the nominal plant are shown on Fig. 7. First, Figs. 7a and 7b show that the controller does not cancel the lightly damped zeros and poles of the plant. This interesting characteristic is the result of two different factors. On the one hand, the coprime factors H_∞ synthesis avoids an exact cancellation.[9] It is known that the problem solved in that case involves a four block criterion.[5] Nevertheless, preliminary experiments with the coprime factorization procedure on the satellite show that the controller almost cancels the plant if special care is not taken. On the other hand, introducing an inner loop slightly changes the location of the nominal plant poles. This avoids cancellation of the actual poles of the plant.

Singular value Bode plots of the output sensitivity, Fig. 7c, and complementary sensitivity, Fig. 7d, lead to the computation of satisfying multivariable output margins. Input margins are quite similar.

Output margins:

$$\begin{aligned} MG &=]-15.6 \quad 10.9[\text{dB} \\ MP &= \pm 49\,\text{deg} \end{aligned} \tag{14a}$$

Input margins:

$$\begin{aligned} MG &=]-15.6 \quad 12.7[\text{dB} \\ MP &= \pm 49\,\text{deg} \end{aligned} \tag{14b}$$

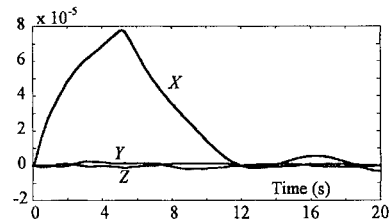

a) Angular position (rad)

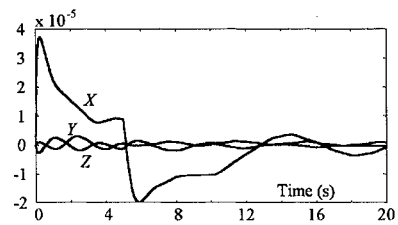

b) Angular rate (rad/s)

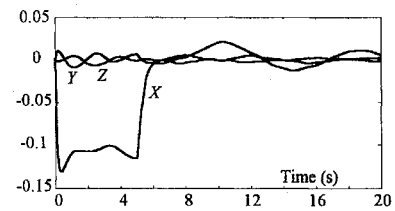

c) Control torque (Nm)

Fig. 8 Responses to an EMS disturbance on X axis.

Time Responses

The more complete DYCEMO linear models of the satellite are used for a first evaluation of the design using SIMULINK. The EMS disturbance and the gyro noise are applied to different models, corresponding to different panel positions. Figures 8 and 9 give an example of the results obtained, which clearly meet the specifications given in Sec. II. In addition, they can be favorably compared with results obtained using other modern control techniques.[1,2]

Results for the Y axis or Z axis are similar to those obtained for the X axis. Finally, all plots of Fig. 8 indicate that good decoupling properties are obtained between the three axes (X, Y, and Z).

μ Analysis

Using the more recent version of the MATLAB toolbox[15] μ analysis is then performed to check the stability robustness of the control law against uncertainties in the natural frequencies of the flexible modes. Only uncertainties in modes 1, 2, 3, 5, and 7 were considered. The other modes are less excited by the control law and are known to have practically no effect on stability degradation.

To perform such an analysis, the closed-loop system of Fig. 6 is put into the standard form of Fig. 10, where all uncertainties are incorporated in the matrix Δ. This model is obtained from Eqs. (1) and (2) by introducing parameter uncertainties in the C and K matrices

$$I_G\ddot{\theta}_G + L_G^T\ddot{\eta} = C_{\text{ext}} \tag{15}$$

$$\ddot{\eta} + \left(I + P^T S_r\,\Delta_r\,P\right)C\dot{\eta} + \left(I + P^T S_r\,\Delta_r\,P\right)^2 K\eta = -L_G\ddot{\theta}_G \tag{16}$$

with

$$P = \begin{pmatrix} 1 & 0 & 0 & 0 & 0 & 0 & 0 & 0 \\ 0 & 1 & 0 & 0 & 0 & 0 & 0 & 0 \\ 0 & 0 & 1 & 0 & 0 & 0 & 0 & 0 \\ 0 & 0 & 0 & 0 & 1 & 0 & 0 & 0 \\ 0 & 0 & 0 & 0 & 0 & 0 & 1 & 0 \end{pmatrix}$$

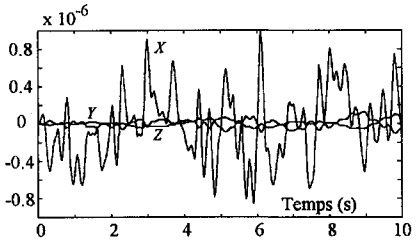

Fig. 9 Rate responses to gyro noise on X axis.

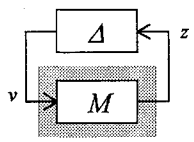

Fig. 10 Standard diagram for μ analysis.

to select modes 1, 2, 3, 5, and 7, and $S_r = \text{diag}\{s_i\}$ to scale the uncertainty in each frequency. The 5×5 uncertainty matrix is $\Delta_r = \text{diag}\{\delta_i\}$ with $\delta_i \in [-1\ +1]$. Such a model allows the frequency of mode i to take any value between $\omega_{ci}(1 - s_i)$ and $\omega_{ci}(1 + s_i)$, where ω_{ci} is the nominal value.

The last term in the left-hand member of Eq. (16) is linearized using a first-order approximation:

$$\ddot{\eta} = -L_G\ddot{\theta}_G - C\dot{\eta} - K\eta - P^T S_r\,\Delta_r(PC\dot{\eta} + 2PK\eta) \tag{17}$$

and the uncertainty model can be obtained by building the block diagram corresponding to Eqs. 15 and 17 (Fig. 11). However, it is well known[16] that analysis with only real uncertainties is difficult to solve because of continuity and convergence problems. A procedure has been proposed[15,16] to replace real uncertainties by uncertainties with a small complex part.

Another technique has been used in this paper. Complex uncertainties were introduced in a physical manner by considering inverse multiplicative uncertainty $\Delta_c = \text{diag}\{\delta_{c1}; \delta_{c2}; \delta_{c3}\}$, $\delta_{ci} \in \boldsymbol{C}$, $|\delta_{ci}| < 1$, at the control input of the plant, with scaling factor $s_c \in \boldsymbol{R}$ (Fig. 11). Complex uncertainties $s_c\Delta_c$ can be viewed as gain and phase uncertainties acting on each output of the controller. More precisely, s_c can be interpreted as the radius of a circle centered on point (-1), which is to be avoided by the Nyquist plot of each open-loop control channel with the other channels closed and the other uncertainties considered. The block diagram of Fig. 11 is then obtained, where the gray area represents the matrix M, and uncertainties are modeled as $\Delta = \text{diag}\{\Delta_r; \Delta_c\}$.

The mixed real/complex structured singular value was then computed by considering the following scaling factors:

$$s_1 = 0.3 \quad s_2 = 0.3 \quad s_3 = 0.3 \quad s_5 = 0.25 \quad s_7 = 0.25 \tag{18}$$

which correspond to 30% uncertainty on frequencies of modes 1, 2, and 3, and 25% on modes 5 and 7. Plots of the upper bound of $\mu[M(j\omega)]$ given by the algorithm proposed in Ref. 15 are represented in Fig. 12, for five different solar array configurations. Each frequency has been considered with its nominal value so that each model is different from the synthesis model of Table 2 (depending on the plots, the scaling factor s_c on complex uncertainties is taken between 0.03 and 0.05; 1000 frequency points were computed around each mode to make sure that no peak was forgotten).

As shown in Fig. 12, the maximal value of $\mu[M(j\omega)]$ is 1.06 (obtained for the 45-deg model). It can be deduced that the closed-loop system remains stable for any $|\delta_i|$ and $|\delta_{ci}|$ less than 1/1.06, i.e., for the following uncertainties: $\pm 28.3\%$ on frequencies of modes 1, 2, and 3 and $\pm 23.6\%$ on frequencies of modes 5 and 7. Furthermore, since the lower bound algorithm proposed in Ref. 15 did not converge in this application, these values are suspected to be somewhat conservative. Implementation results (see Sec. V) show that

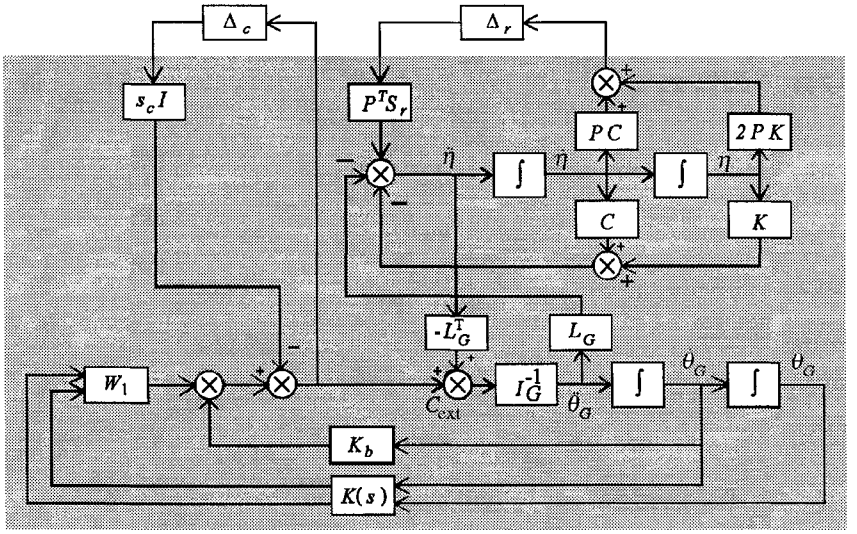

Fig. 11 Block diagram μ analysis of SPOT4 control law.

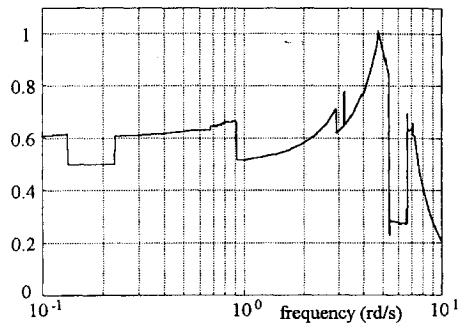

a) 0-deg solar array configuration

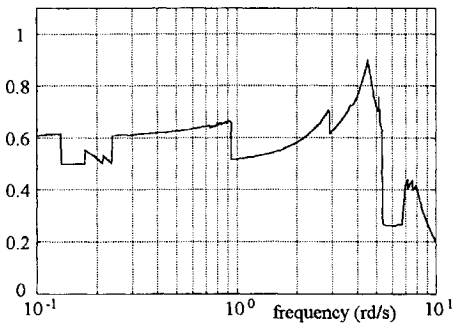

c) 90-deg solar array configuration

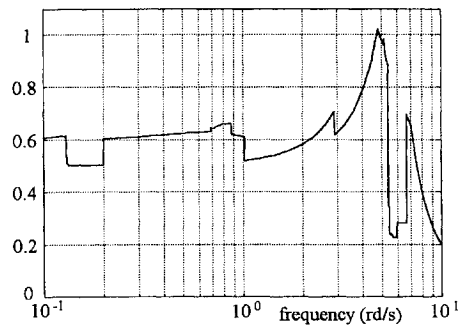

b) 45-deg solar array configuration

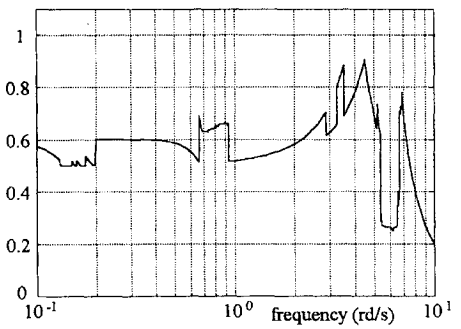

d) 135-deg solar array configuration

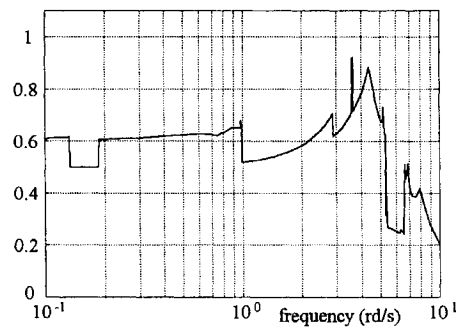

e) 180-deg solar array configuration

Fig. 12 Upper bound plots of the structured singular value.

stability is maintained for higher deviations than the ones deduced by μ analysis.

Discrete-Time Synthesis

A digital controller is required for the satellite with 8-Hz sampling frequency. There are two ways to obtain such a controller. A bilinear transform can be applied to the continuous-time controller or a discrete H_∞ synthesis can be performed. The second solution is preferred because the bilinear transform introduces high-frequency distortion when the sampling frequency is not sufficiently large with respect to the closed-loop bandwidth, as is the case here.

A great advantage of using the coprime factors H_∞ method is that the discrete-time synthesis is no more difficult than the continuous-time one. The solutions are obtained by solving two LQG type discrete Riccati equations.[10,11]

Only constant matrices were used for K_b and W_1 in the continuous-time case. This structure is maintained for discrete-time synthesis (Fig. 13): K_b and W_1 are identical to the ones used in the continuous-time case [see Eqs. (11) and (12)]. The maximum stability margin is $\varepsilon_{\max} = 0.575$ and the controller is computed for $\varepsilon = 0.99\varepsilon_{\max}$. The equivalent controller has 28 state variables, which is identical to the continuous-time controller.

The singular value Bode plots and the time responses are not shown because the results are similar to those presented in the continuous-time case.

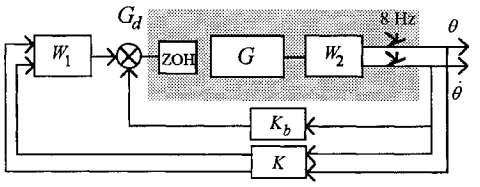

Fig. 13 Control structure: discrete-time synthesis.

V. Implementation

The linear evaluation of the H_∞ design has been shown to be promising, and a digital controller is available. However, it is necessary to check these results at a higher level. The 28 state H_∞ digital controller is implemented in the complete nonlinear simulation program of MMS. The main objective of this stage is to evaluate the robust performance of the design in the presence of nonlinearities and throughout the entire orbit of the satellite.

First, Fig. 14 illustrates the behavior of SPOT4 with respect to an EMS disturbance. Position and torque of the X axis are shown, with the disturbance having negligible effects on the Y and Z axes. These results are almost identical to the ones obtained in Fig. 11. The maximum position error is 8×10^{-5} rad, whereas the maximum value of the control torque is 0.18 Nm. The responses are well damped and little affected by the gyro noise.

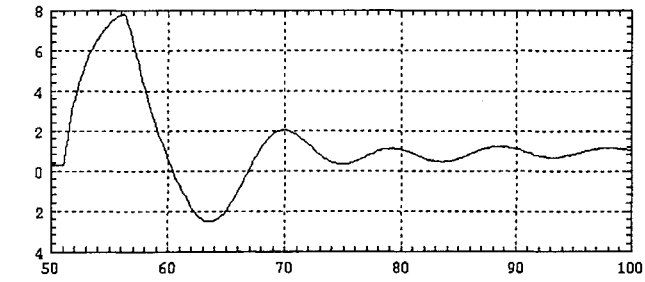

a) Angular position (10^{-5} rad) vs time (s)

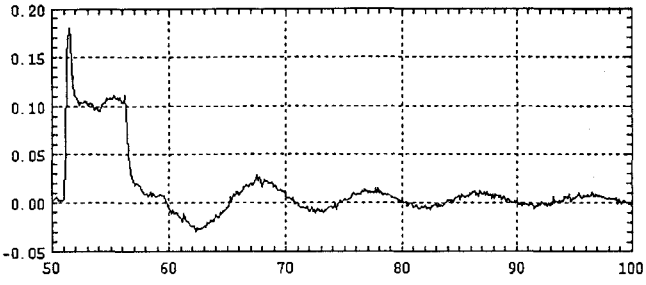

b) Control torque (Nm) vs time (s)

Fig. 14 EMS disturbance responses.

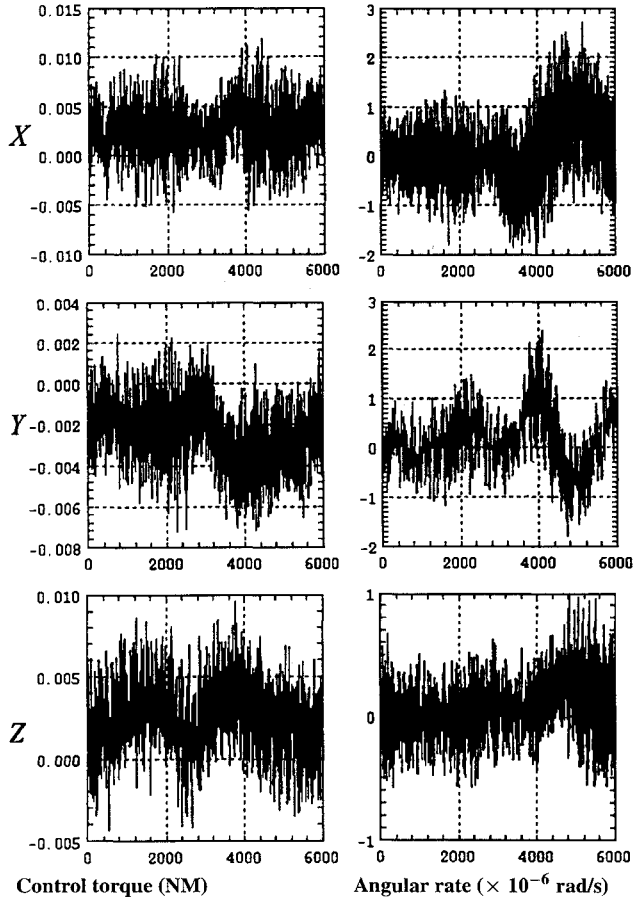

Fig. 15 Ideal simulation throughout the orbit.

Results throughout the entire orbit are plotted in Fig. 15, without gyro noise. To better understand these results, a statistical analysis has been performed (Table 3). The rate errors and the control torques remain below the specifications given in Sec. II, with significant margins.

The behavior with respect to gyro noise has been similarly analyzed. The degradation with respect to the ideal case is about 12% for the rate error and 70% for the control torque.

Finally, robustness of the control law has been checked by performing simulations with different values for the parameters of the plant. Instability was never detected. The worst-case results have been obtained for the following parameters: ω_{c1} and ω_{c2} at +20%, ω_{c3}–ω_{c7} at −30%, central body inertia lowered within 15%, central body mass lowered within 5%, and gyro filters parameters chosen so that the phase is maximum. The degradation with respect to the previous case is only 9% for the rate error and only 6% for the control torque.

Table 3 Statistical analysis for ideal simulation

	Rate error 3σ rad/s	Control torque 3σ, Nm
X	$2.39\ 10^{-6}$	0.014
Y	$1.94\ 10^{-6}$	0.007
Z	$0.80\ 10^{-6}$	0.008

As the linear analysis predicts, the nonlinear time simulations have confirmed that the satellite is stabilized by a unique fixed H_∞ controller throughout the orbit. The performances obtained meet the design specifications. In addition, they are satisfying, as compared with previously designed control laws.[1,2]

VI. Conclusion

This paper has presented results concerning the robust stabilization of an Earth observation satellite from the SPOT family. The satellite model contains zeros and poles with very low damping, parameter uncertainties, and dynamics variations.

Using a combination of a collocated rate feedback and the loop shaping design procedure of McFarlane and Glover,[5] a unique controller was synthesized stabilizing the satellite throughout the entire orbit. The collocated rate feedback was used to precondition the plant, shrinking the uncertainty ball and therefore reducing the sensitivity of the inner loop. Constant compensators were then introduced to shape the singular values of the plant, resulting in a satisfactory stability margin. Finally, robust stabilization of the shaped plant provided the controller.

The robustness of the control law has been ensured by using μ analysis. The concept of inner loop is very important since it allowed the controller to be implemented without gain scheduling and also avoided cancellation of the low damped plant poles and zeros by the controller. This latter fact is a key point for robustness.

Both linear analysis and full dynamics nonlinear simulations have shown satisfactory behavior and improvements with respect to other control laws. The only disadvantage is the high order obtained using H_∞ synthesis. Further studies will investigate the possibility of significantly reducing the controller order without damaging the robustness, by using a combination of reduction procedure and μ analysis.

Acknowledgments

This research has been supported by the Centre National d'Études Spatiales, under Contract 896/CNES/92/1668/00, with the participation of MMS.

References

[1]Champetier, C., Desplats, E., and Pelipenko, P., "Modern Control Techniques for Spacecraft AOC/GNC Systems," *Proceedings of the 1st ESA International Conference on Spacecraft Guidance, Navigation, and Control Systems* (Noordwijk, The Netherlands), 1991, pp. 483–490.

[2]Charmeau, M.-C., and Pelipenko, P., "New Methods for New Challenge in Spacecraft Control Design," *Proceedings of the 12th IFAC Symposium on Automatic Control in Aerospace* (Ottobrunn, Germany), 1992, pp. 491–496.

[3]Le Ballois, S., "Commande H_∞ Multivariable d'un Satellite par les Facteurs Premiers, Assurant la Robustesse vis-à-vis des Modes Souples," Ph.D. Thesis, Univ. of Paris-Sud and Supélec, Feb. 1994.

[4]Frapard, B., Le Ballois, S., Champetier, C., and Duc, G., "Méthodes de Commande Multivariable Robustes pour Satellite d'Observation. Rapport Final," CR 896/CNES/92/1668/00, Nov. 1994.

[5]McFarlane, D., and Glover, K., "Robust Controller Design Using Normalized Coprime Factor Plant Descriptions," *Lecture Notes in Control and Information Sciences*, Springer–Verlag, Berlin, 1990.

[6]Zames, G., "Feedback and Optimal Sensitivity, Model Reference Transformations, Multiplicative Seminorms and Approximate Inverses," *IEEE Transactions on Automatic Control*, Vol. 26, No. 2, 1981, pp. 301–320.

[7]Doyle, J. C., Glover, K., Khargonekar, P. P., and Francis, B. A., "State-Space Solutions to Standard H2 and H_∞ Control Problems," *IEEE Transactions on Automatic Control*, Vol. 34, No. 8, 1989, pp. 831–846.

[8]Glover, K., and McFarlane, D., "Robust Stabilization of Normalized Coprime Factors Plant Description with H_∞-Bounded Uncertainty," *IEEE Transactions on Automatic Control*, Vol. 34, No. 8, 1989, pp. 821–830.

[9]Sefton, J., and Glover, K., "Pole/Zero Cancellations in the General H_∞ Problem with Reference to a Two Block Design," *Systems and Control Letters*, Vol. 14, No. 4, 1990, pp. 295–306.

[10]Walker, D. J., "Robust Stabilizability of Discrete-Time Systems with Normalized Stable Factor Perturbation," *International Journal of Control*, Vol. 52, No. 2, 1990, pp. 441–455.

[11]Walker, D. J., and Postlethwaite, I., "Discrete-Time H_∞ Control Laws for a High Performance Helicopter," Robust Control System Design Using H_∞ and Related Methods Symposium, Univ. of Cambridge, England, UK, March 1991.

[12]Iglesias, P. A., and Glover, K., "State-Space Approach to Discrete-Time H_∞ Control," *International Journal of Control*, Vol. 54, No. 5, 1991, pp. 1031–1073.

[13]Safonov, M. G., Chiang, R. Y., and Flashner, H., "H_∞ Robust Control Synthesis for a Large Space Structure," *Journal of Guidance, Control, and Dynamics*, Vol. 14, No. 3, 1991, pp. 513–520.

[14]Chiang, R. Y., Safonov, M. G., Haiges, K., Madden, K., and Tekawy, J., "A Fixed Controller for a Supermaneuverable Fighter Performing the Herbst Maneuver," *Automatica*, Vol. 29, No. 1, 1993, pp. 111–127.

[15]Balas, G. J., Doyle, J. C., Glover, K., Packard, A., and Smith, R., "μ-Analysis and Synthesis Toolbox," Math Works Inc., 1993.

[16]Packard, A., and Pandey, P., "Continuity Properties of the Real/Complex Structured Singular Value," *IEEE Transactions on Automatic Control*, Vol. 38, No. 3, 1993, pp. 415–428.